MICRO-RAMAN ANALYSIS OF IRRADIATED DIAMOND FILMS

Robert L. Newton
ED36A, Marshall Space Flight Center
Huntsville, AL 35812

Telephone: 256-544-7880, 256-544-5877 (fax)
robby.newton@msfc.nasa.gov

ABSTRACT

Owing to its unique and robust physical properties, diamond is a much sought after material for use in advanced technologies, even in Microelectromechanical Systems (MEMS). The volume and weight savings promised by MEMS-based devices are of particular interest to spaceflight applications. However, much basic materials science research remains to be completed in this field. Results of micro-Raman analysis of proton (10^{15} – 10^{17} H^+/cm^2 doses) irradiated chemical vapor deposited (CVD) films are presented and indicate that their microstructure is retained even after high radiation exposure.

INTRODUCTION

Diamond possesses many of the most sought after material properties desired in present day manufacturing. Its extreme hardness, high wear resistance, chemical inertness, optical transparency, and wide band-gap serve to illustrate this fact. As Figure 1 demonstrates, crystalline diamond has the highest elastic modulus and hardness values known (1).
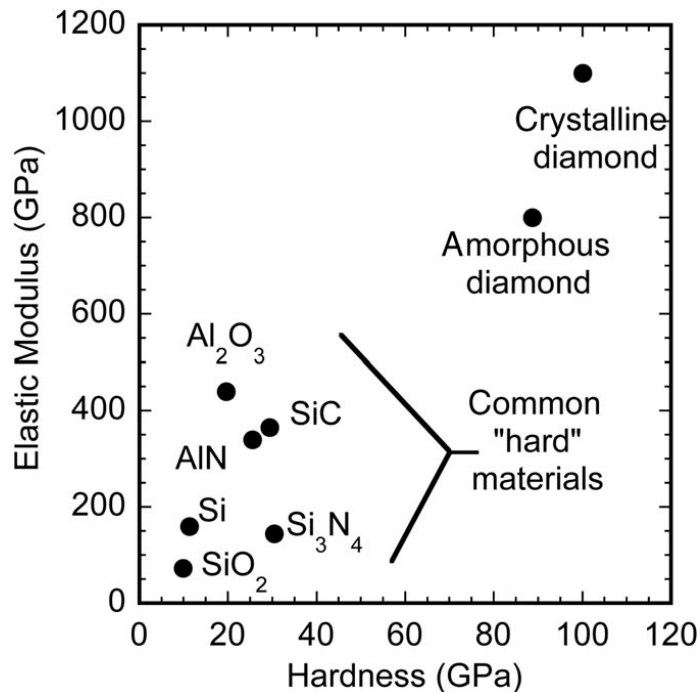

Figure 1. Comparison of hardness and elastic modulus values for a variety of "hard" engineering materials.

Synthetic 'Industrial diamond' has been commercially prepared for over thirty years yet it is polycrystalline diamond produced by techniques such as chemical vapor deposition (CVD) that show the greatest promise for insertion into advanced technologies such as electronics (2), MicroSystems (MST), and MicroElectroMechanical Systems (MEMS). In the rapidly growing areas of MST and MEMS technologies, recent work has demonstrated that diamond-based MEMS devices are feasible (3,4). Diamond offers significant advantages over silicon, the material currently used most often, especially in harsh environments such as high temperature or where high specific stiffness is required (5,6). Questions continue to be raised about silicon's durability in applications where high wear rates are involved.[7]

The understanding and control of film stress is a very important issue facing MEMS devices. MEMS materials should exhibit residual stresses of less than 10Mpa. This becomes even more significant for high modulus materials such as diamond. In diamond, the above stress level corresponds to an elastic strain of about 0.00001. This is equivalent to about 1Å of displacement for every 10 microns of beam length, assuming uniform loading. Of equal importance are strain gradients throughout the thickness of the film (8).

Diamond's resistance to radiation damage may prove to be one of its most valuable assets, especially for uses where exposure to potentially harmful radiation will be the norm, not the exception. Yet unlike silicon and most other materials, both single crystal and polycrystalline diamond have a tendency to convert to a physically very different, but compositionally identical, material upon sufficient irradiation…that being graphite. This is not surprising since graphite is the more thermodynamically stable form of carbon. Due to the large differences in the mechanical properties of these carbon polymorphs and the importance of understanding stress states in this material, it is important to characterize and understand this radiation-induced phenomenon, especially if the diamond film is to be used for structural purposes in MEMS/MST applications.

There are three major sources of ionizing radiation in the low-earth (LEO)/near earth environment: galactic cosmic rays, energetic electrons and protons trapped in the Earth's radiation belts, and solar particle events. However, protons and electrons dominate the radiation environment. The energy and Flux values for protons and electrons are given in Table 1(9).

Table 1. Particle type, energy and flux for LEO and near-Earth space environment.

Particle	Energy (p/cm^2-day)	Flux (p/cm^2-day)
Electron	100 keV-50MeV	10^2-10^{10}
Proton	100keV-10^3MeV	10^6-10^{10}

The goal of this investigation was to examine the relationship between proton dose and microstructure in chemical vapor deposited (CVD) diamond films using specimens mounted cross-sectionally. The use of protons allows one to not only study the charged particle that may cause the most microstructural damage in earth-orbit MEMS devices but also allows the study of relatively deeply buried damage inside the diamond material without resorting to MeV implant energies that may create extensive damage via the high energy needed for the implantation process itself. Since MEMS devices operating in space will not possess an opportunity to reverse radiation damage via annealing, only non-annealed specimens were investigated. Two high spatial resolution techniques – Scanning Electron Microscopy (SEM) and micro-Raman Spectroscopy (micro-Raman) were used to examine these relationships.

EXPERIMENTAL PROCEDURE

Polycrystalline diamond of approximately 20 microns in thickness was prepared at Vanderbilt University on a 2" single crystal silicon substrate by using microwave plasma assisted chemical vapor deposition (MPACVD) at a temperature of 800°C and a pressure of 110 Torr. The hydrogen flow rate was 479 sccm, methane flow rate was

18 sccm with a microwave power of 5 kilowatts. The total time of film deposition was twenty hours. Figure 2 illustrates a cross-sectional view of the as-deposited wafer.
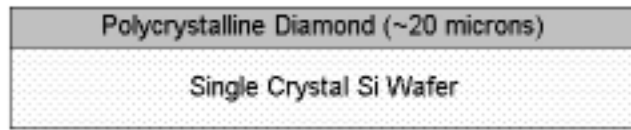

Figure 2. Schematic (cross-section) of polycrystalline diamond thin film prepared by microwave plasma-assisted chemical vapor deposition (MPACVD). The diamond is grown directly on the silicon substrate.

The samples were implanted with protons using a NEC Model 5SDH-2 Pelletron accelerator located at Alabama A&M University in Huntsville Alabama. 600KeV protons were implanted to dosages of $2 \times 10^{15} H^+/cm^2$, $2 \times 10^{16} H^+/cm^2$, and $2 \times 10^{17} H^+/cm^2$, respectively, at room temperature. Based on theoretical calculations (TRIM software) this energy should deposit protons to a depth of ~4 microns into the films (10). The irradiation rate was kept below $10^{13} H^+/cm^2/sec$ so that non-linear effects could be avoided. After irradiation, the samples were cut and mounted on edge. They were then polished by personnel at both the Marshall Space Flight Center in Huntsville, AL and by personnel at the Oak Ridge National Laboratory in Oak Ridge, TN. SEM micrographs of the specimens were taken using an ElectroScan Environmental SEM located at the Marshall Space Flight Center in Huntsville, AL. Raman spectra were collected at Oak Ridge National Laboratories with a Dilor XY800 Raman microprobe (JY, Inc., Edison, NJ) configured as a single stage spectrograph using the microscope with a ~1 micron resolution. An Innova 308C Ar^+ ion laser (Coherent, Inc., Santa Clara, CA) at 514.5 nm and 100 mW output power was used to excite the sample.

EXPERIMENTAL RESULTS

The diamond specimens were all taken from one 2" wafer. A composite photograph of all the specimens after each implantation regime is presented in Figure 3. The outline of the beam is visible in both the $2 \times 10^{16} H^+/cm^2$ and $2 \times 10^{17} H^+/cm^2$ implants.
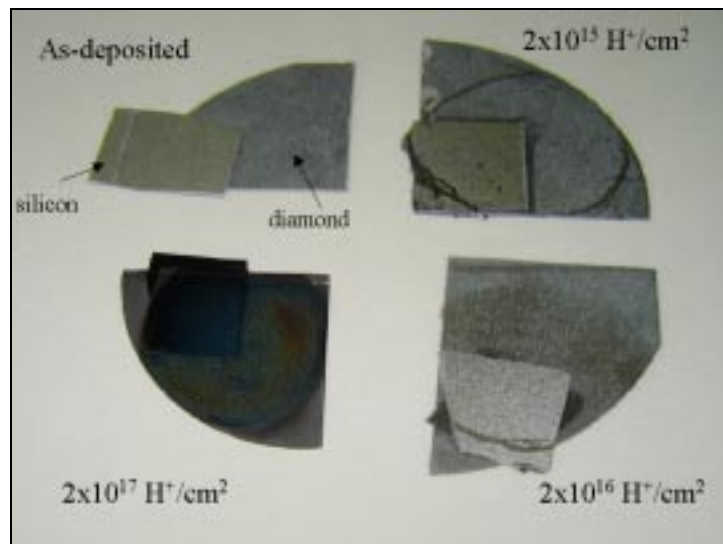

Figure 3. Photograph showing all specimens used in this investigation. The black lines on two of the samples were used to outline the beam diameter. Polycrystalline silicon specimens were also irradiated but results not presented in this paper.

No visible changes were observed in the $2x10^{15}$ H^+/cm^2 implant. For the $2x10^{16}$ H^+/cm^2 specimen, a mark was made on the surface of the specimen to delineate all of the irradiated area. Noticeable darkening was observed on the diamond specimen. The $2x10^{17}$ H^+/cm^2 implanted specimen was visibly much different than the as-deposited sample. Due to space limitations, the experimental data from the two mid-level implantations is not presented although some discussion of the experimental results for these are presented in the text.

Scanning Electron Microscopy (SEM) analysis was performed on all un-mounted specimens, examining both the top surfaces and the cleaved edges. Only the results from the as-deposited and most heavily irradiated specimens are presented herein. Prior to SEM analysis, all samples were rinsed with acetone, which was immediately blown off with compressed air. However, debris remained on the surface of all specimens. This debris was examined by x-ray fluorescence spectroscopy and was identified as being composed of elements such as Ca, K, and S although qualitative determination was not possible. Since the debris was present on all specimens, the material could not have been introduced via the implantation process. Also, this debris was absent on SEM analysis of the edge of the diamond specimens. As such, this debris was classified as surface contamination only. The top surface of the as-deposited diamond specimen indicated a <111> crystal growth with large facets. The grains are on the order of several microns in diameter with sharp, well defined edges. An SEM micrograph of the as-deposited specimen is shown in Figure 4. The top surface of the $2x10^{15}$ H^+/cm^2 implanted specimen appeared to be identical to the as-deposited material. No visible change in the surface of the diamond was detected. Careful inspection of the top surface of the $2x10^{16}$ H^+/cm^2 implanted specimen indicated that although the crystallites remained intact, dark regions randomly populate the micrograph. However, the edges of the crystals remained well defined.

The situation is significantly different for the $2x10^{17}$ H^+/cm^2 implanted material, that being the most heavily irradiated specimens. The wide-angle and close-up micrographs indicate severe degradation of the crystallite edges…so much so that the grains have a somewhat "melted" appearance. A close-up SEM micrograph is shown in Figure 5.
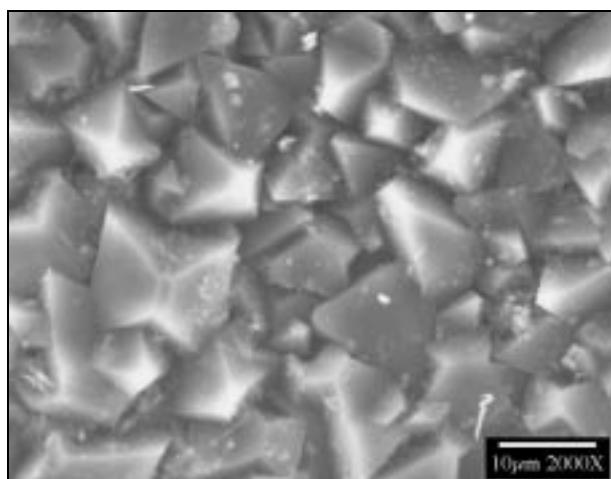

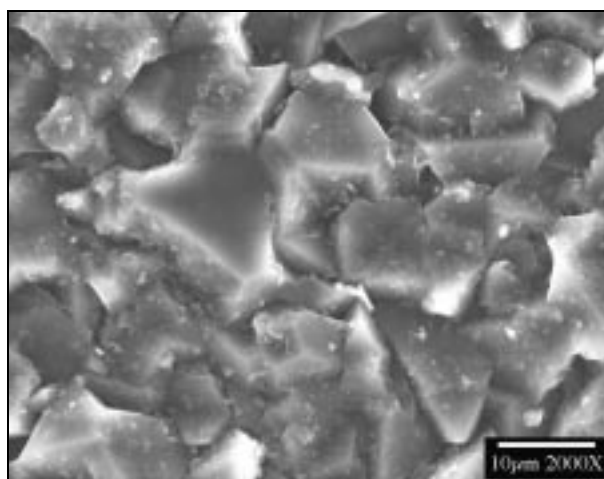Figure 4. Scanning Electron Micrograph (SEM) of top surface of "as-deposited" polycrystalline diamond film.

Figure 5. Scanning Electron Micrograph (SEM) of top surface of $2x10^{17}$ H^+/cm^2 proton implanted polycrystalline diamond film.

Raman spectra were collected in triplicate from the top surface of each specimen. While the penetration depth of the Raman laser signal will vary with opacity, surface roughness, laser energy, etc., the signal does penetrate several microns into the material (11). The spectra have been averaged, smoothed and normalized. A Lorentzian function was used for curve fitting and an example is shown in the inset for the "as-deposited" spectra (see Figure 6). Single crystal diamond exhibits a sharp Raman peak at ~1333 cm^{-1} with a Full Width at Half Maximum (FWHM) of less than 3.0 with no other spectral signatures present. The as-deposited material compared extremely well with high purity single crystal material, although the diamond used in this study was polycrystalline.

The diamond peak is sharp, well defined and symmetrical. The FWHM is close that that reported for high-purity single crystal material (~3 cm^{-1}). No graphitic or amorphous bands are observed. The Raman spectra for the diamond specimen irradiated with a proton dose of $2x10^{15}$ H$^+$/cm^2 compared favorably with the as-deposited material. The FHWM was slightly lower, but within experimental error for the as-deposited sample. No graphitic components were detected. The diamond peak is sharp, well defined, and symmetrical, indicating no measurable microstructural damage from the irradiation. The intensity of the peak matched very closely that of the as-deposited specimen. The Raman spectra from the top surface of the $2x10^{16}$ H$^+$/cm^2 implant began to show some effects from the implantation. Since a slight amount of darkening was present in this sample, the probe depth of the laser is reduced with respect to the as-deposited and $2x10^{15}$ H$^+$/cm^2 implanted samples. While the diamond peak is sharp, intense, and largely symmetrical, the peak is shifted slightly downward, indicating tension within the microstructure. The slight increase in the FWHM, taken with the 1630cm^{-1} peak present in the spectra, suggests that ion-induced defects are responsible.

The spectra taken from the top surface of the most heavily irradiated specimen indicates extensive ion-induced damage to the microstructure(see Figure 7). Due to the extreme darkening of the surface of this specimen, the probe depth of the Raman signal is attenuated in comparison to the as-deposited and $2x10^{15}$ H$^+$/cm^2 implanted samples. The first-order diamond peak is shifted downward by almost two wavenumbers. The intensity of the peak is greatly diminished. The FWHM broadening is due to the ion-induced defects which are observed from ~1490 to 1650 cm^{-1}. Peaks attributed to ion-implantation damage - i.e. the monovacancy (1490cm^{-1}), the split interstitial (1630cm^{-1}), and the broad graphitic band at ~1550cm^{-1}, are observed. Other damage related peaks are also observed. However, the sharp line located ~1430cm^{-1} is due to a detector malfunction within the Raman system.
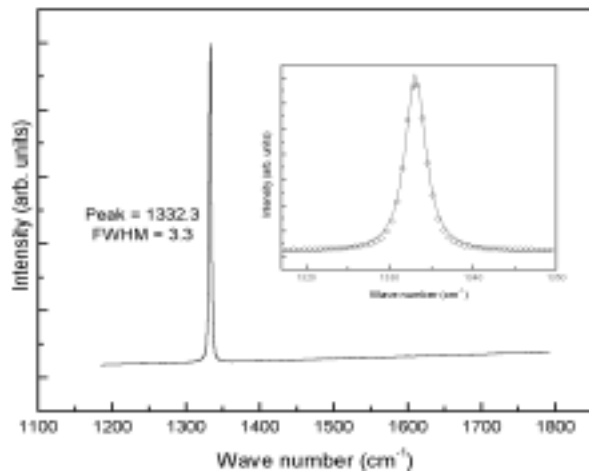

Figure 6. Micro-Raman spectra of top surface of "as-deposited" polycrystalline diamond wafer. Inset shows Lorentzian fit to experimental data.
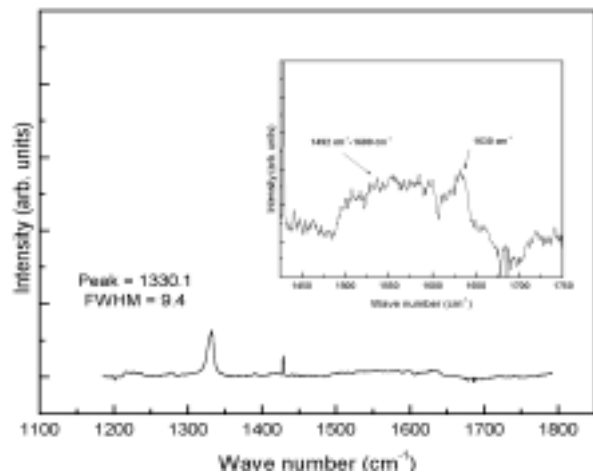
Figure 7. Micro-Raman spectra of top surface of $2x10^{17}$ H$^+$/cm^2 implanted polycrystalline diamond wafer. Implantation induced damage is shown in inset.

Figure 8 presents an overview of the top surface micro-Raman investigation. The first order Raman peak position and the first order peak FWHM are examined in relationship to proton dosage. With respect to the first order diamond peak position, within experimental error, the as-deposited and $2x10^{15}$ H$^+$/cm^2 implanted specimens are very similar to each other. The $2x10^{16}$ H$^+$/cm^2 and $2x10^{17}$ H$^+$/cm^2 implanted samples reveal increasing damage with increasing proton dosage. However, the first order diamond peak was still evident. This is not surprising since the greatest amount of microstructural damage is expected to occur near the end of range (EOR) of the implant,

which in this case is ~4 microns deep, and not near the surface of the material where the majority of the Raman signal originates from within the sample.

The FWHM follows a similar patter for these series of implantations. While the $2x10^{16}H^+/cm^2$ implant reveals a slight broadening, indicating microstructural damage, the $2x10^{17}H^+/cm^2$ implant indicates a much larger shift. Also, the as-deposited and $2x10^{15}H^+/cm^2$ implants were, within experimental error, unaffected by the irradiation.
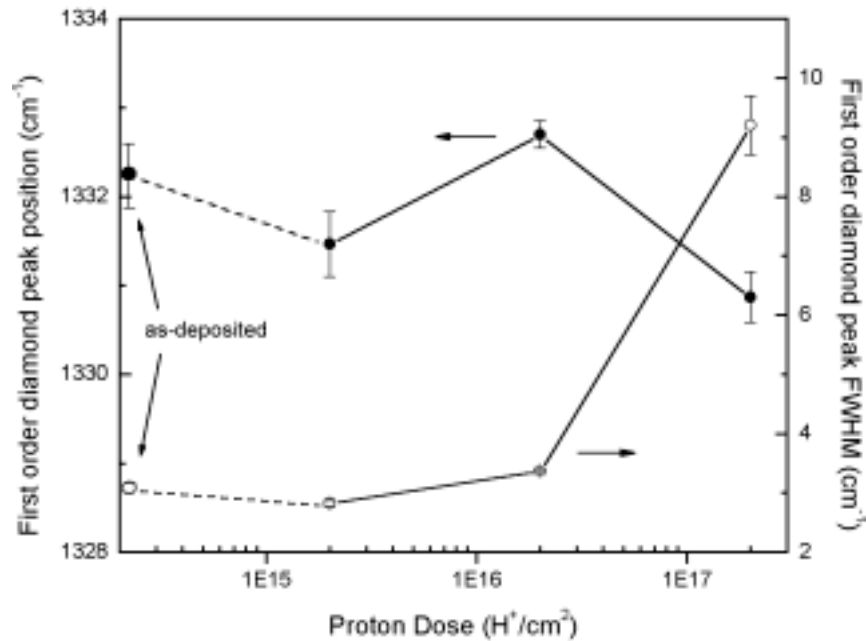
Figure 8. Graph showing first order diamond peak position and first order diamond peak Full Width at Half Maximum (FWHM) as a function of proton dosage for entire series.

After SEM analysis of the top surfaces of the diamond specimens, they were then examined along the fractured edges. This was done in order to visually examine any depth dependent effects the proton implantation might have created. The results of this investigation are shown in Figures 9 and 10 for the as-deposited and heavily irradiated specimens, respectively. SEM edge analysis of the as-deposited material revealed an extremely rough edge surface. The interface of the diamond film/silicon substrate is clearly evident. Columnar grain growth, typically seen in <111> diamond films, is difficult to detect in this specimen. The $2x10^{15}$ H^+/cm^2 implanted film edge looks much like the as-deposited material. No radiation damage, either on the surface or down the edge, is observed in any of the specimens.
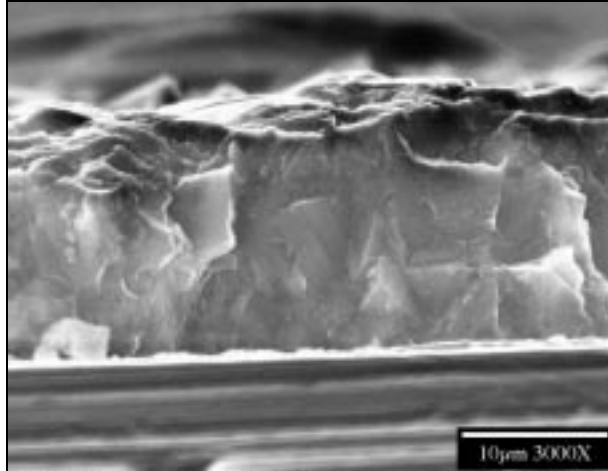
Figure 9. SEM micrograph showing the edge surface of the "as-deposited" polycrystalline diamond wafer. The diamond film/silicon substrate interface is indicated by the white horizontal line near the lower portion of the figure.
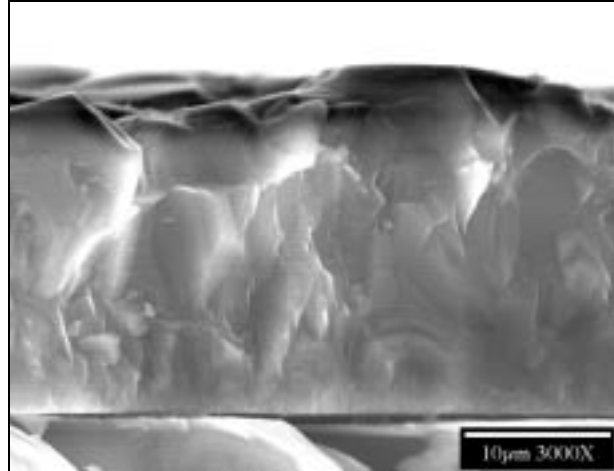
Figure 10. SEM micrograph showing the edge surface of $2x10^{17}$ H^+/cm^2 implanted polycrystalline diamond wafer.

Raman spectra were obtained on both unpolished and polished diamond specimens. No artifacts from the polishing were observed. However, since the polished specimens did provide a more uniform surface for investigation, they were used for the high resolution data collection.

The micro-Raman spectra were collected by performing a "line scan" across the specimen cross-section. Each "line scan" consisted of forty individual spectra that were collected at intervals of every micron. The scan would start on the silicon substrate and end past the edge of the sample. Since silicon and diamond have very different Raman signatures, locating the interfaces of the films was relatively simple. However, this was complicated due to the fact that near the films interfaces, the Raman spot size included contributions from both the silicon and diamond.

The spectra for the as-deposited material is shown in Figure 11. The 1um line scan contains a sharp first-order diamond peak at ~1332 cm^{-1}. However, the broad band from ~1450 to 1700 cm^{-1} is indicative of graphitic-like carbon. This is attributed to surface effects, were carbon exists in a variety of bonding configurations. The 2-6 micron scans are void of this broad peak signifying the high fidelity of the carbon film throughout the entire layer. This material appears to be free of depth-dependent stress and microstructural damage due to the fact that the first-order diamond peak shifted very little nor was there an increase in the FWHM.

The line scans for the $2x10^{15}$ H^+/cm^2 implanted specimen looked similar to the control specimen. The depth-dependent Raman line scans for the $2x10^{16}$ H^+/cm^2 implanted specimen revealed a defect-related peak at 1630 cm^{-1}. This defect is associated with the <100> split interstitial. This peak increased with depth and reached a maximum at 4 microns, beyond which it decreased rapidly and was absent at 6 microns. Also, there was a slight increase in the baseline between the regions of 1400 cm^{-1} and the 1630 cm^{-1} peak.

The proton implantation effect as a function of depth for the most heavily irradiated specimen, the $2x10^{17}$ H^+/cm^2 implant, is presented in Fig. 12. In this representative line scan series, extensive defect-related spectral signatures are evident even at 1um. The vacancy (1495 cm^{-1}), the broad amorphous region at ~1550 cm^{-1}, and the <100> split interstitial (1630 cm^{-1}) are all present. The first order Raman line is greatly diminished in intensity as compared to the control sample. The damage increases until reaching a maximum at 4 microns. At this depth, the diamond peak is diminished in intensity but still present. The 1495 cm^{-1} peak may be present but resolution is impossible due to the increase in baseline present throughout this entire region. The 1630 cm^{-1} peak grows in intensity as a function of depth until reaching a maximum at 4 microns as well. By 6 microns, the spectra returned

7

in appearance to looking very similar to the as-deposited specimen, although the baseline is still slightly elevated across the entire 1400 cm^{-1} to 1650 cm^{-1} region.
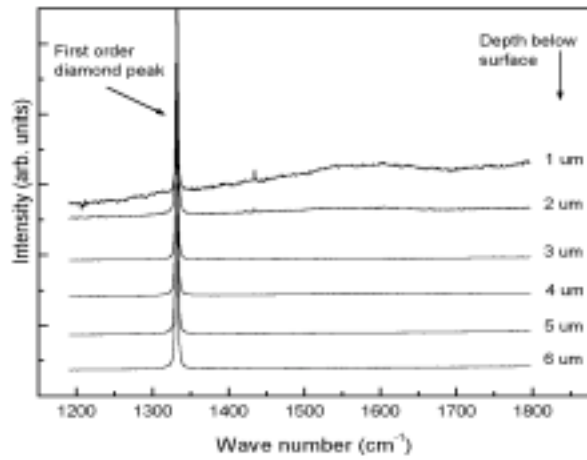

Figure 11. Micro-Raman spectra as a function of depth across the surface of the "as deposited" polycrystalline diamond film.
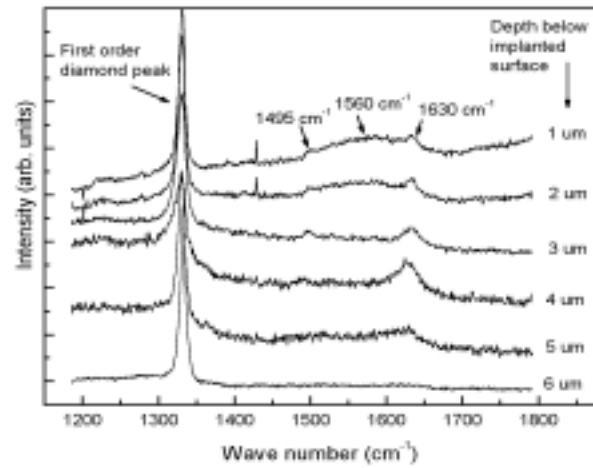
Figure 12. Micro-Raman spectra as a function of depth across the surface of the $2 \times 101^{7}H^{+}/cm^{2}$ polycrystalline diamond film.

Summary charts are presented in Figures 13 and 14 for the entire diamond series. First order diamond peak position is seen to shift for both the 2×10^{16} H^{+}/cm^{2} and the 2×10^{17} H^{+}/cm^{2} implant series. Likewise, the FWHM variation as a function of depth illustrates an increasing damage to the microstructure until reaching a maximum at the End of Range (EOR). This is to be expected due to the fact that the maximum carbon atom displacement occurs near the end of the proton travel where a maximum of nuclear energy is deposited. Past the EOR, a slow return to baseline is observed. In applications where extremely low stress/strain values in the film are critical, this effect could affect device performance.
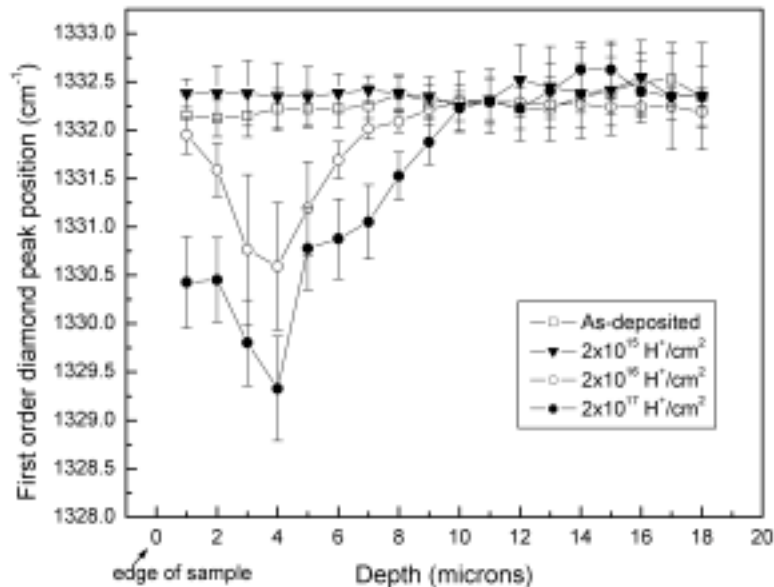

Figure 13. Variation in first order peak position as a function of depth for the entire series.
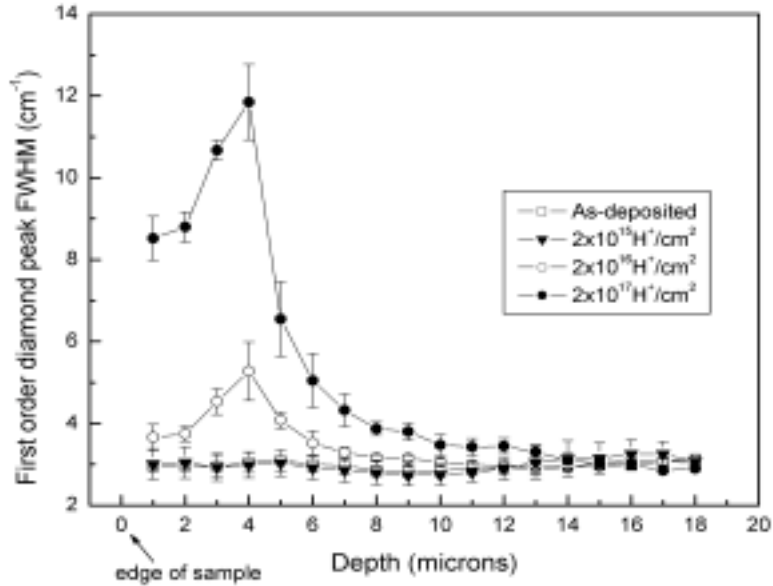
Figure 14. Variation in first order FWHM as a function of depth for the entire series.

CONCLUSIONS

The effects of proton irradiation on CVD diamond films have been examined using SEM and micro-Raman techniques. A proton dose of $2x10^{17}H^+/cm^2$ is sufficient to visibly darken and degrade the top surface of the films. Raman analysis indicated both a shift in first order diamond peak position and FWHM. These conditions indicate both stress and microstructural damage near the surface of the films.

In the cross-sectional analysis, TRIM software accurately predicted the implantation range of the protons. Across the series, the maximum peak shift and FWHM broadening occurred at ~4 microns from the surface. The damage increased with increasing dosage although the first order diamond peak was always present, implying that the diamond structure was not totally destroyed by the implantation.

ACKNOWLEDGEMENTS

1. Sullivan, J.P., Friedman, T.A., and Hjort, K., MRS Bulletin, April 2001.

2. Railkar, T.A., et. al., Critical Reviews in Solid State and Materials Science, 25(3), 163, (2000).

3. Davidson, J.L., Kang, W.P., Gurbuz, Y., Holmes, K.C., Davis, L.G., Wisitsora-at, A., Kerns, D.V., Eidson, R.L., and Henderson, T., D., Diamond Relat. Mater. 8 , 1741 (1999).

4. Kohn, E., Gluche, P., and Adamschik, M., Diamond Relat. Mater. 8, 934 (1999).

5. Spearing, S.M., Acta. Mater. 48, 179 (2000).

6. Fahrner, W.R., Job, R., and Werner, M., Microsystem Technologies 7, 138, (2001).

7. Wang, et. al., Sensors & Actuators A, 97-98, 486, 2002.

8. Sullivan, J.P., Friedman, T.A., and Hjort, K., MRS Bulletin, April 2001.

9. NASA-MSFC Internal Technical Publication (1999).

10. Ziegler, J.F., Biersack, J.P., and Littmark, U., The Stopping and Range of Ions in Matter, Pergamon Press, New York, 1985.

11. Private communication with Dr. M. Lance, Oak Ridge National Labs.